Optica Applicata, Vol. XXXVIII, No. 2, 2008

Ray tracing method in a 3D analysis of fiber-optic elements

J.S. WITKOWSKI*, A. GROBELNY

Wrocław University of Technology, Institute of Telecommunications, Teleinformatics and Acoustics, Wybrzeże Wyspiańskiego 27, 50-370 Wrocław, Poland

*Corresponding author: jerzy.witkowski@pwr.wroc.pl

In this paper, a numerical analysis of algorithm of optical fiber systems with dimensions much larger than light wavelength has been presented. This algorithm can be used especially in the case of multimode fiber-optic elements. The presented technique of the analysis is based on the ray tracing method (RTM). Up to now, the RTM was widely used for an analysis of lens-systems. In this paper, a new possibility for this method in fiber optic elements analysis has been shown. The algorithm permits to determine thousands of ray traces simultaneously in a desired 3D area of an arbitrarily defined refractive index. This technique can be applied for a gradient index (GI), step index (SI) fibers, different types of optical couplers, *etc*. The algorithm has been extended to analyze dispersion properties and pulse shape evolution tracking along a fiber-optic system.

Keywords: dispersion, optical fiber system, optical, pulse evolution, ray tracing method.

1. Introduction

Different types of analysis of optical systems have been developed for many years. Most of algorithms are described in a comprehensive way in [1]. This book treats analytical and numerical methods including the finite element method, finite difference method, and various kinds of beam propagation methods (BPM).

In this paper, authors have shown that in the case of large aperture systems, including multimode fiber optic systems of a large modal number (hundreds and thousands), the RTM (geometrical optics) based on Fermat's principle [2] can be effectively utilized. This method is not treated in the mentioned reference [1] but is worthy of consideration. Until now, the RTM was widely used in commercial optical system design programs for lens-systems analysis. In contrast, this paper presents the new usage of the method used for fiber optics elements analysis. The examples, shown in the paper, prove the usefulness of RTM.

2. Ray tracing algorithm

Utilized in the paper, the ray tracing method (RTM) assumes that light wavelength is infinitesimal ($\lambda = 0$). This assumption leads to the so-called "geometrical optics", in which a light ray runs along a path called *trajectory* or *ray trace* [2]. Equation for the ray trace can be derived from Fermat's principle which says that the path of a ray of light between two points $p_1(x_1, y_1, z_1)$ and $p_2(x_2, y_2, z_2)$ minimizes the travel time,

$$T = \int_{p_1}^{p_2} \frac{\mathrm{d}s}{u(x, y, z)} \tag{1}$$

where $u(x, y, z)$ is a speed of light (*full version of Fermat's Principle states that the optical path length must be extreme* [3, 4]). In this equation, ds represents the elementary step of a ray path. The speed of light $u(x, y, z)$ in the medium of refractive index $n(x, y, z)$ can be expressed by $u = c/n$ (c – speed of light in vacuum). Minimization of the above equation by Euler–Lagrange method leads to the following equation:

$$\frac{\mathrm{d}}{\mathrm{d}s}\left[n(x, y, z)\frac{\mathrm{d}\mathbf{R}}{\mathrm{d}s}\right] = \mathrm{grad}(n) \tag{2}$$

where: ds – elementary section of trajectory, n – refractive index, $\mathbf{R}$ – positional vector of the ray (Fig. 1).

Figure 1 explains that d$\mathbf{R}$/ds is a unit vector directed along the ray path and can be written as

$$\frac{\mathrm{d}\mathbf{R}}{\mathrm{d}s} = [\cos\alpha, \cos\beta, \cos\gamma] = \mathbf{A} \tag{3}$$

where: α, β, γ – angles between the direction of a ray path and x, y, z – axis respectively.

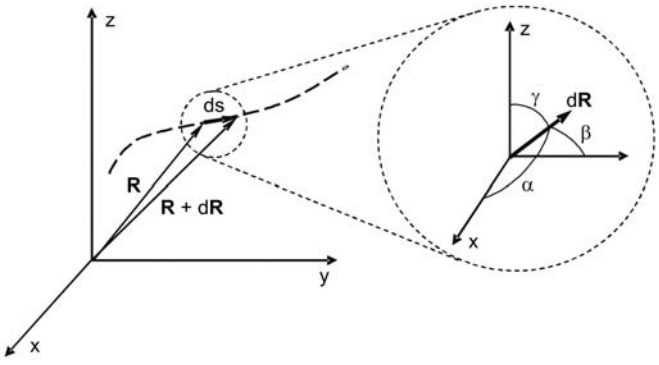

Fig. 1. Explanation of vector spatial symbols in Eq. (2).

Equation (2) can be now rewritten in the following form:

$$n\frac{\mathrm{d}\mathbf{A}}{\mathrm{d}s} = \mathrm{grad}(n) - \mathbf{A}\frac{\mathrm{d}n}{\mathrm{d}s} \tag{4}$$

where dn/ds is a derivation of the refractive index n in the direction of ds that can be expressed as

$$\frac{\mathrm{d}n}{\mathrm{d}s} = \mathbf{A}\,\mathrm{grad}(n) \tag{5}$$

Combining (4) and (5) we have

$$\frac{\mathrm{d}\mathbf{A}}{\mathrm{d}s} = \frac{1}{n(x, y, z)}\left[\mathrm{grad}(n) - \mathbf{A}\left(\mathbf{A}\,\mathrm{grad}(n)\right)\right] \tag{6}$$

where

$$\mathrm{grad}(n) = \left[\frac{\partial n}{\partial x}, \frac{\partial n}{\partial y}, \frac{\partial n}{\partial z}\right] = \left[n_x, n_y, n_z\right] \tag{7}$$

Equation (6) can be rewritten in the form below:

$$\begin{aligned}
\frac{\mathrm{d}(\cos\alpha)}{\mathrm{d}s} &= \frac{1}{n}\left\{n_x - \left(\left[n_x, n_y, n_z\right]\cdot\left[\cos\alpha, \cos\beta, \cos\gamma\right]\right)\cos\alpha\right\} \\
\frac{\mathrm{d}(\cos\beta)}{\mathrm{d}s} &= \frac{1}{n}\left\{n_y - \left(\left[n_x, n_y, n_z\right]\cdot\left[\cos\alpha, \cos\beta, \cos\gamma\right]\right)\cos\beta\right\} \\
\frac{\mathrm{d}(\cos\gamma)}{\mathrm{d}s} &= \frac{1}{n}\left\{n_z - \left(\left[n_x, n_y, n_z\right]\cdot\left[\cos\alpha, \cos\beta, \cos\gamma\right]\right)\cos\gamma\right\}
\end{aligned} \tag{8}$$

The standard approach to the above written equation consists of the left-hand side manipulations to achieve angles α, β, γ and use them as integration variables. In the algorithm presented, the authors use $\cos\alpha$, $\cos\beta$, $\cos\gamma$ as integration variables.

Introducing finite differences, instead of derivative, Eq. (8) becomes

$$\begin{aligned}
&\mathrm{d}(\cos\alpha) \to (\cos\alpha)_{k+1} - (\cos\alpha)_k \\
&\mathrm{d}(\cos\beta) \to (\cos\beta)_{k+1} - (\cos\beta)_k \\
&\mathrm{d}(\cos\gamma) \to (\cos\gamma)_{k+1} - (\cos\gamma)_k \\
&\mathrm{d}s \to \Delta s
\end{aligned} \tag{9}$$

where the subscript k denotes the integration step, and Δs is a finite elementary integration step. The final numerical algorithm can be expressed in the form

$$(\cos\alpha)_{k+1} = \left(\frac{1}{n}\left\{n_x - \left(\left[n_x, n_y, n_z\right]\cdot\left[\cos\alpha, \cos\beta, \cos\gamma\right]\right)\cos\alpha\right\}\right)_k \Delta s + (\cos\alpha)_k$$

$$(\cos\beta)_{k+1} = \left(\frac{1}{n}\left\{n_y - \left(\left[n_x, n_y, n_z\right]\cdot\left[\cos\alpha, \cos\beta, \cos\gamma\right]\right)\cos\beta\right\}\right)_k \Delta s + (\cos\beta)_k \tag{10}$$

$$(\cos\gamma)_{k+1} = \left(\frac{1}{n}\left\{n_z - \left(\left[n_x, n_y, n_z\right]\cdot\left[\cos\alpha, \cos\beta, \cos\gamma\right]\right)\cos\gamma\right\}\right)_k \Delta s + (\cos\gamma)_k$$

Because the vector $[\cos\alpha, \cos\beta, \cos\gamma]$ is a unit vector

$$\cos^2\alpha + \cos^2\beta + \cos^2\gamma = 1 \tag{11}$$

so the equation system (10) and (11) is overdetermined and one of the expressions in Eqs. (10) can be omitted.

In practice, the algorithm Eq. (10) has been modified to the subsequent form:

$$(\cos\alpha)_{k+1} = \left(\frac{1}{n}\left\{n_x - \left(\left[n_x, n_y, n_z\right]\cdot\left[\cos\alpha, \cos\beta, \cos\gamma\right]\right)\cos\alpha\right\}\right)_k \Delta s + (\cos\alpha)_k$$

$$(\cos\beta)_{k+1} = \left(\frac{1}{n}\left\{n_y - \left(\left[n_x, n_y, n_z\right]\cdot\left[\cos\alpha, \cos\beta, \cos\gamma\right]\right)\cos\beta\right\}\right)_k \Delta s + (\cos\beta)_k \tag{12}$$

$$(\cos\gamma)_{k+1} = \sqrt{1 - (\cos\alpha)^2_{k+1} - (\cos\beta)^2_{k+1}}$$

The last expression in Eq. (12) assumes that $\cos\gamma$ is always greater or equal to zero. In the case of fiber optic systems analysis, where the z-axis is directed along the fiber – the γ angle is relatively small, the assumption is always satisfied (only the forward propagation is analyzed).

Finally, the ray path (ray position in the system) can be expressed in the following form:

$$\begin{aligned} x_{k+1} &= x_k + \Delta s\cos\alpha \\ y_{k+1} &= y_k + \Delta s\cos\beta \\ z_{k+1} &= z_k + \Delta s\cos\gamma \end{aligned} \tag{13}$$

Simultaneously with the light ray travel, time along the analyzed optical system can be summed up:

$$T_{k+1} = T_k + \frac{\Delta s}{u} = T_k + \frac{\Delta s}{c / n(x, y, z)} \tag{14}$$

This new feature of the presented algorithm gives a possibility to calculate fiber system dispersion properties.

Examining travel times of a large number of rays enables us to estimate dispersion properties of the fiber system or even observe the evolution of a pulse shape propagated in the fiber.

To complete the derivations, it should be explained that in the algorithm, the refractive index n is calculated in a uniform mesh $\{x_i, y_j\}$ with a grid $\Delta x = \Delta y = 0.5$ μm for each z_k. The value n between the grid nodes is taken as a linear interpolation of $n(\{x_i, y_j, z_k\})$:

$$\begin{aligned} n(x, y, z) = & \frac{n(x_i + \Delta x, y_j, z_k) - n(x_i, y_j, z_k)}{\Delta x}(x - x_i) \\ & + \frac{n(x_i, y_j + \Delta y, z_k) - n(x_i, y_j, z_k)}{\Delta y}(y - y_j) \\ & + \frac{n(x_i, y_j, z_k + \Delta z) - n(x_i, y_j, z_k)}{\Delta z}(z - z_k) \end{aligned} \tag{15}$$

$$\begin{aligned} & x_i + \Delta x \geq x > x_i \\ & y_j + \Delta y \geq y > y_j \\ & z_k + \Delta z \geq z > z_k \end{aligned} \tag{15a}$$

For so defined distribution of the refractive index n, the function grad(n) can be obtained as a finite difference:

$$\begin{aligned} \text{grad}(n) &= \left[n_x, n_y, n_z \right] \\ &= \left[\frac{n(x + \delta x, y, z) - n(x, y, z)}{\delta x}, \frac{n(x, y + \delta y, z) - n(x, y, z)}{\delta y}, \frac{n(x, y, z + \delta z) - n(x, y, z)}{\delta z} \right] \end{aligned} \tag{16}$$

where, in the below presented examples, $\delta x = \delta y = \delta z = 0.5$ μm were chosen (in general, Δ and δ can be chosen differently).

It should be emphasized that the presented algorithm applies geometrical optics and can be used for large diameter fibers. RTM does not take into account the phase, polarization and back scattering that are neglected for the presented examples.

3. Examples of analysis

The following part of the paper presents the results of the analysis of two types (GI and SI) of fibers. The refractive index profile for SI fiber has been defined as

$$n(r) = n_{co}\left\{1 + \frac{n_{co} - n_{cl}}{n_{co}} \exp\left[-\left(\frac{r^2}{R_{co}^2}\right)^{20}\right]\right\} \tag{17}$$

where: n_{co} – core refractive index, n_{cl} – clad refractive index, R_{co} – core radius, r – radius.

The exponential part simulates the realistic shape of the refractive index in the step index fiber. The power 20 in this expression has been chosen to achieve a total change of the refractive index in the thickness of 5 μm (Fig. 2).

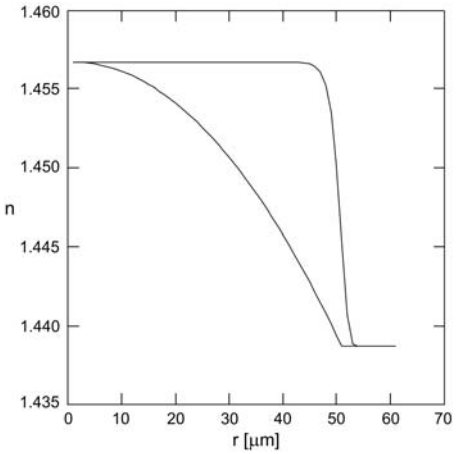

Fig. 2 . Refractive index profiles $n(r)$ for both GI and SI analyzed fibers.

The main advantage of such an approach is that the function $n(x, y, z)$ is continuously differentiable, particularly on the border between the core and the clad.

GI fiber was assumed to have a truncated square-law [5] profile defined by

$$n(r) = \begin{cases} n_{co}\left(1 - 2\Delta n \dfrac{r^2}{R_{co}^2}\right)^{0.5} & \text{for} \quad r \le R_{co} \\ n_{cl} & \text{for} \quad r > R_{co} \end{cases} \tag{18}$$

where:

$$\Delta n = \frac{n_{co}^2 - n_{cl}^2}{2n_{co}^2} \tag{19}$$

The refractive index profiles $n(r)$ for both types of fibers are shown in Fig. 2. As seen, the differences in the core and the clad refractive index are the same for GI and SI fibers. The core refractive index has been taken $n_{co} = 1.4567$ (silica glass refractive index). The core radius $R_{co} = 50$ μm has been chosen for both fibers.

The example of rays' paths for GI and SI fibers are shown in Fig. 3.

In Figure 4, a few ray paths in two types of fiber couplers, made with the polishing technique, are shown. The profiles of the refractive index are the same as in the previous examples described by Eqs. (17) and (18).

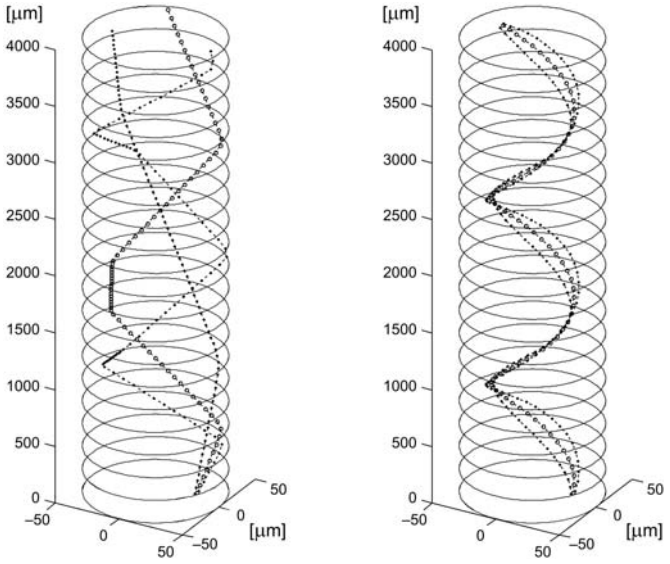

Fig. 3. Examples of ray paths in GI and SI fibers.

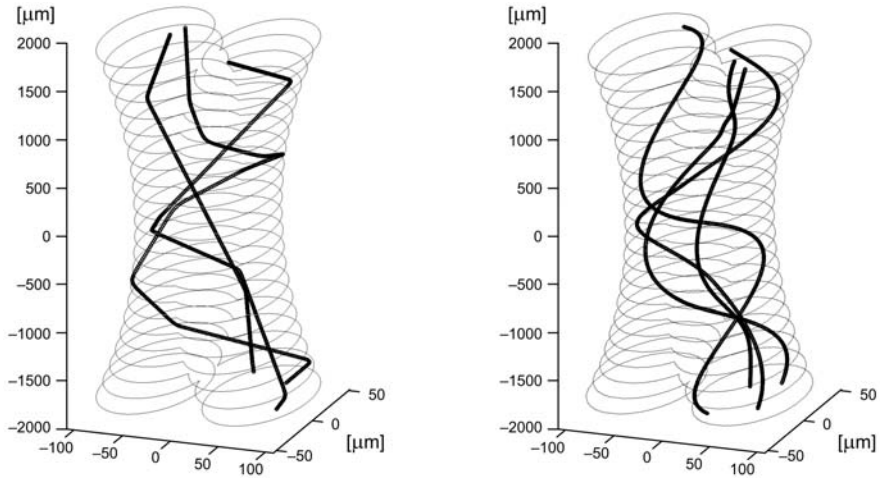

Fig. 4. Ray paths in GI and SI fiber couplers made using polishing technique.

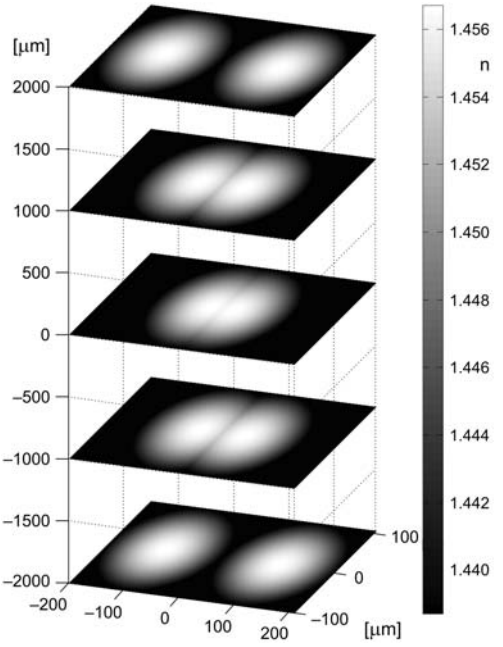

Fig. 5. Refractive index profile for the coupler made with GI fibers employing polishing method.

In Figure 5, the refractive index profile for the coupler made with GI fibers Eq. (18) is shown. The described algorithm allows us to determine such parameters as a coupling ratio and an attenuation ratio of fiber couplers. More practical results were presented in [6, 7].

As seen, the described algorithm can be used to analyze 3D systems where the refractive index $n(x, y, z)$ is a function of not only the radius but z-axis as well.

Estimating of the numerical aperture (NA) for an arbitrary fiber is yet another possibility of the above algorithm. Figure 6 illustrates a few ray paths that are lunched into the center of a fiber at different angles γ, ($\alpha = 90°$ – see Fig. 1). Through an analysis of propagated and leaked rays, it is possible to determine NA. The predicted from the above algorithm values of NA are accurate up to the fourth decimal digit when compared to the precise analytical solution

$$\mathrm{NA} = \sqrt{n_{\mathrm{co}}^2 - n_{\mathrm{cl}}^2} = \sqrt{1.4567^2 - 1.4387^2} = 0.2283 \tag{20}$$

In the next part of the paper, the authors have studied modal dispersion and power density in a cross section of the fiber. Calculations have been performed for the clad radius R_{cl} equal to 100 μm, and refractive index profiles as in previous Eqs. (17), (19). Through analyzing positions of a large number of rays propagated in the fiber (in presented examples 5000) for the desired cross section, it is possible to calculate the ray density, which corresponds to the power density of the conducted light in this cross section. In this way, it is possible to obtain power density as the function of z.

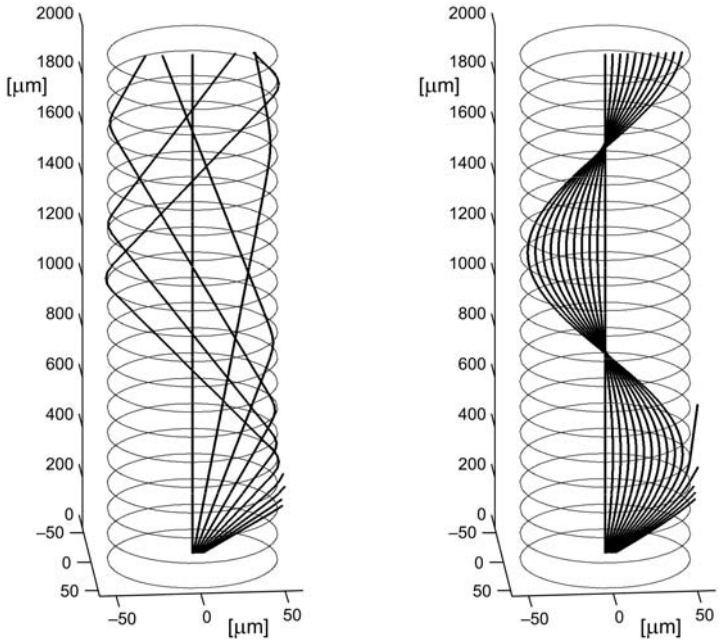

Fig. 6. Light ray paths in GI and SI fibers allowed to determine numerical aperture (NA).

Presented in Fig. 7, ray travel times correspond to a pulse shape for a given z under assumption that the fiber is excited with an infinitely short pulse. For presented results, the calculated dispersion with respect to 1 km and 90% of power is 0.43 ns/km. Analogical results for the fiber of a different length (0.1 cm shorter) are shown in Fig. 8. A very significant difference in the power density and the pulse shape can be seen. In this case, the calculated dispersion is equal to 0.50 ns/km. Differences in

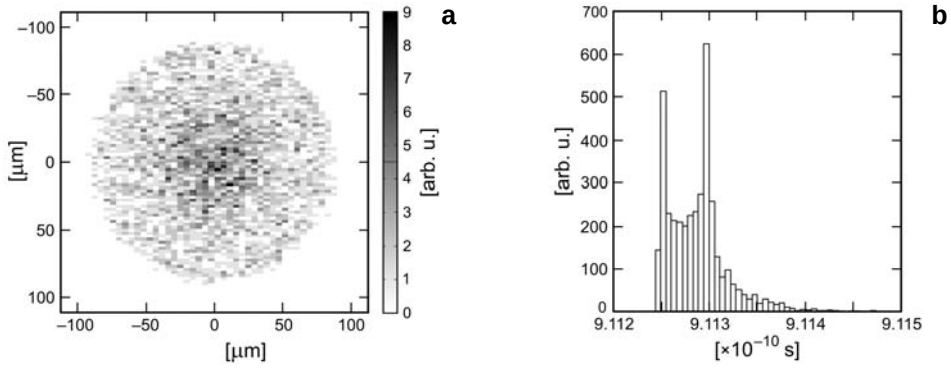

Fig. 7. Power density in the GI fiber at $z = 18.22$ cm and for uniform excitation at $z = 0$ cm (**a**). The histogram of ray travel times (calculated dispersion with respect to 1 km and 90% power is 0.43 ns/km) (**b**).

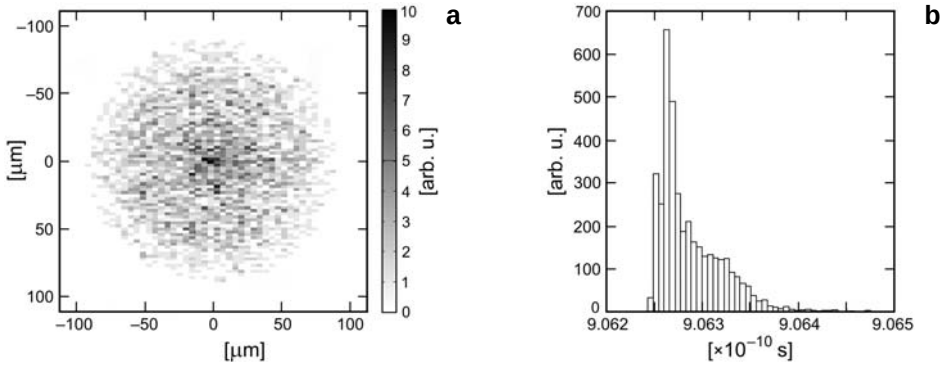

Fig. 8. Power density in the GI fiber at $z = 18.12$ cm and for uniform excitation at $z = 0$ cm – **a**. The histogram of ray travel times (calculated dispersion with respect to 1 km and 90% power is 0.50 ns/km) – **b**.

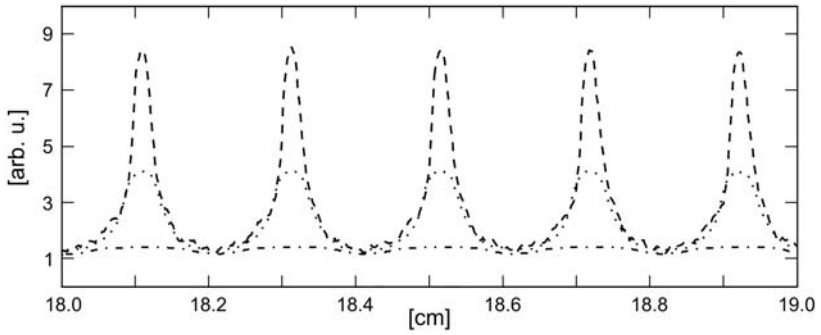

Fig. 9. Profile of relative power density $P(r)$ for GI fiber according to (21) for $r = 0.14R_{co}$ (– – –), $r = 0.3R_{co}$ (•••), $r = 0.8R_{co}$ (– • –); R_{co} – core radius.

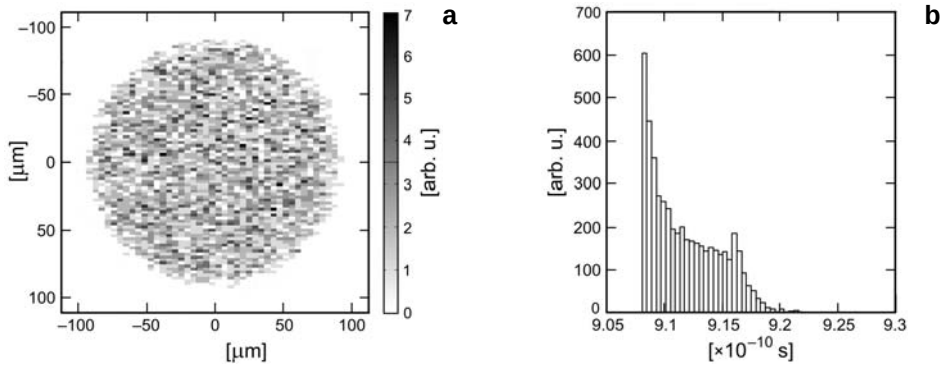

Fig. 10. Power density in the SI fiber at $z = 17.99$ cm and for uniform excitation at $z = 0$ cm – **a**. The histogram of ray travel times (calculated dispersion with respect to 1 km and 90% power is 50 ns/km) – **b**.

the pulse shape and the dispersion for both cases result from the feature of GI fiber and lie in the power density changes along the fiber (compare Fig. 7**a** and Fig. 8**b**).

The periodical changes of the power density in the GI fiber is presented in Fig. 9, where the power density in the fiber cross section obtained as the ratio of the power contained in a circle of radius r to the surface of the circle has been analyzed. The relative power density defined as:

$$P(r) = \frac{\int_0^r \int_0^{2\pi} p(r, \Theta) r \, \mathrm{d}\Theta \mathrm{d}r}{\pi r^2} \left(\frac{\int_0^R \int_0^{2\pi} p(r, \Theta) r \, \mathrm{d}\Theta \mathrm{d}r}{\pi R^2} \right)^{-1} \tag{21}$$

(r – radius, R – radius of core, $p(r, \Theta)$ – power distribution) is shown in Fig. 9.

Due to periodical changes of the power density (Fig. 9), a calculated dispersion for different cross sections can differ more than 20%. This difference comes from a different shape and width of pulses for different lengths of the analyzed fiber. The specific pulse shape in Fig. 7**b** (with two maxima) gives the similar result, such as that obtained with different computation techniques in [5].

The same analysis has been carried out for the SI fiber (Fig. 10). In this case, the dispersion turned out to be two orders higher in comparison with the GI fiber, and equal to about 50 ns/km. The calculated dispersion is in accordance with the theoretical estimation [8]

$$\Delta\tau = L \frac{n_{\mathrm{co}}}{c} (n_{\mathrm{co}} - n_{\mathrm{cl}}) \approx 87 \text{ ns} \qquad (L = 1 \text{ km}) \tag{22}$$

The presented technique of the ray tracing allows us to analyze ray paths in curved fibers for an arbitrary curvature radius, which corresponds to real situations. Figure 11 shows the power density cross section and the pulse shape in the curved SI fiber.

The calculated dispersion with respect to 1 km turned out to be two times smaller than that for the strait fiber, which is due to a high order mode leakage (mode attenuation). The power density cross section shows the mode shifting to the core–clad border outside the curvature (this is in accordance with intuition). The propagated rays number (Fig. 11**b**) suggests a higher attenuation (bending loss) in comparison with the strait fiber (Fig. 10**b**). The pulse shape is not typical – the rising time is longer than the falling time.

In summary, a curved gradient index fiber has been analyzed (Fig. 12). As in previous examples, the maximum power density is shifted to the outside curvature (Fig. 11**a**), but it keeps a distance from the core–clad border. Dispersions in curved and strait GI fibers are much smaller (Figs. 8 and 12) than those in the case of SI fibers (Figs. 10 and 11).

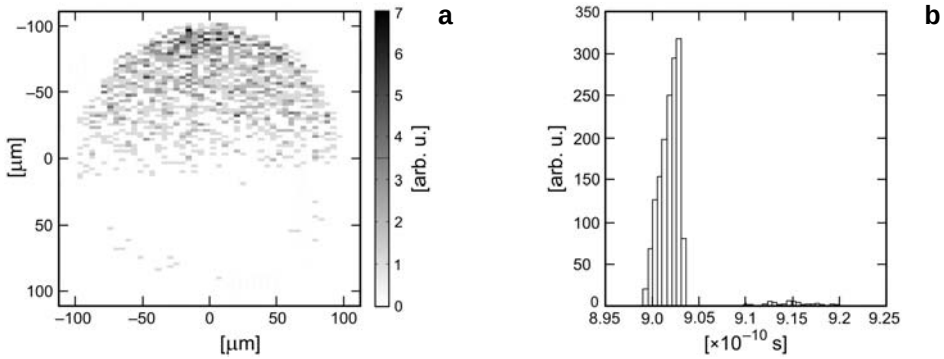

Fig. 11. Power density in the SI curved fiber (R_{cu} = 10 mm) at z = 17.63 cm and for uniform excitation at z = 0 cm – **a**. Rays' travel times histogram (calculated dispersion with respect to 1 km and 90% power is 20 ns/km) – **b**.

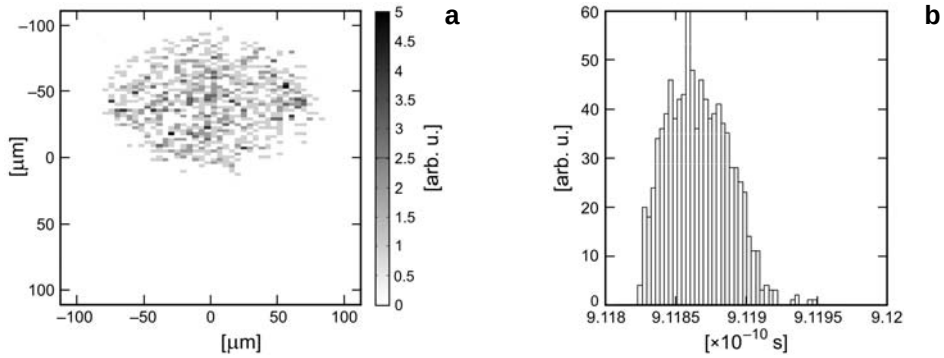

Fig. 12. Power density in the GI curved fiber (R_{cu} = 10 mm) at z = 18.27 cm and for uniform excitation at z = 0 cm – **a**. The histogram of ray travel times (calculated dispersion with respect to 1 km and 90% power is 0.44 ns/km) – **b**.

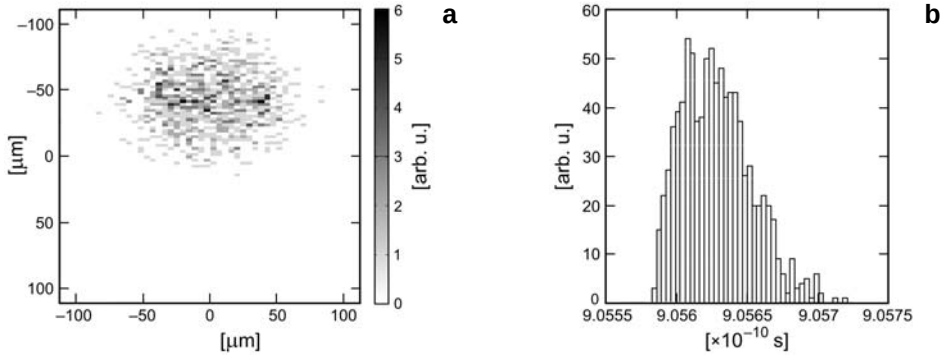

Fig. 13. Power density in the GI curved fiber (R_{cu} = 10 mm) at z = 18.55 cm and for uniform excitation at z = 0 cm – **a**. The histogram of ray travel times (calculated dispersion with respect to 1 km and 90% power is 0.61 ns/km) – **b**.

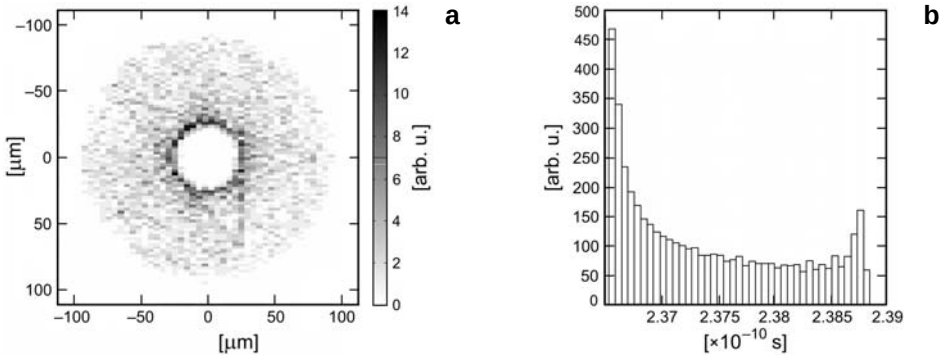

Fig. 14. Power density in the SI fiber for specific uniform excitation at $z = 0$ cm – **a**. The histogram of ray travel times (calculated dispersion with respect to 1 km and 90% power is 48 ns/km) – **b**.

Depending on the analyzed fiber length, the calculated dispersion can be different. Comparison of the results in Figs. 12 and 13 shows that the calculated dispersion differs about 0.2 ns/km when the length of the analyzed fibers differs 3 mm. This result corresponds to a discussion about dispersion differences showed in Figs. 7 and 8.

The calculated dispersion agrees with the theoretical estimation [8]

$$\Delta\tau = L\frac{n_{\mathrm{co}}}{2c}(n_{\mathrm{co}} - n_{\mathrm{cl}})^2 \approx 0.78 \text{ ns} \qquad (L = 1 \text{ km}) \tag{23}$$

It is possible to achieve sophisticated power density profiles for different excitations of the fiber. This result is an effect of lunching the specific group of rays (*that corresponds to subset of modes [5]*) into the SI fiber. One of the examples is shown in Fig. 14.

4. Conclusions

Until now, the ray tracing method was widely used in commercial programs for designing the optical systems, for lens-systems analysis. In contrast, this paper presents a new possibility for this method using an analysis of 3D fiber-optic elements with an arbitrary refractive index profile.

The presented fiber analysis method, based on the ray tracing technique (RTM), turned out to be very effective for the analysis of fiber-optic elements. RTM is based on geometrical optics, so it sets aside interferential phenomena. Still, this method allows us to predict properties of multimode fibers and fiber elements of the diameter much larger than wavelength of transmitted light (mode number – hundreds or more). The implementation of the ray tracing algorithm permits to analyze, in a considerable time, thousands of rays in an optical element. The presented algorithm gives a possibility to design and to describe main features of a number of representative fiber elements (SI or GI), particularly fiber couplers with different geometries and arbitrary refractive index profiles.

The authors would like to emphasize the new feature of the ray tracing algorithm through which it is possible to calculate the dispersion of multimode fiber optic systems. Through an analysis of a large number of rays and their travel time histograms, it is possible to obtain not only dispersion but also observe the evolution of the pulse shape along the fiber as well.

The simulation method presented in the paper is very flexible and can be easily adapted for analyzing different phenomena in fiber optic systems, such as: scattering on impurities in the fiber, a double clad fiber analysis, *etc*.

References

[1] KAWANO K., KITOCH T., *Introduction to Optical Waveguide Analysis: Solving Maxwell's Equations and the Schrödinger Equation*, John Wiley and Sons, New York 2001.

[2] BORN M., WOLF E., *Principles of Optics*, Pergamon Press, Oxford, New York 1968.

[3] FEYNMAN R.P., LEIGHTON R.B., SANDS M., *The Feynman Lectures on Physics*, Vol. 2, Addison Wesley Longman, 1963.

[4] BYRON F.W., FULLER R.W., *Mathematics of Classical and Quantum Physics*, Addison Wesley Pub. Co. Inc. 1969.

[5] ISHIGURE T., KANO M., KOIKE Y., *Which is a more serious factor to the bandwidth of GI POF: Differential mode attenuation or mode coupling?*, Journal of Lightwave Technology **18**(7), 2000, pp. 959–65.

[6] GROBELNY A., WITKOWSKI J.S., BERES-PAWLIK E.M., WÓJCIK J., *A numerical analysis of pumping efficiency using the side coupling method in double-clad fiber lasers*, Proceedings of the SPIE **5951**(1), 2005, pp. 132–7.

[7] GROBELNY A., POWĄZKA P., BACZMAŃSKI J., WITKOWSKI J.S., BEREŚ-PAWLIKI E.M., *Numerical optimisation of side pump-light couplings in power lasers based on double-clad optical fibres*, Proceedings of 2005 7th International Conference on Transparent Optical Networks, Vol. 2, 2005, pp. 355–8 .

[8] EINARSSON G., *Principles of Lightwave Communications*, John Wiley and Sons, New York 1996.

Received March 6, 2007
in revised form October 25, 2007